Supporting Information

Translating Aqueous CO_2 Hydrogenation Activity to Electrocatalytic Reduction with a Homogeneous Cobalt Catalyst

Xinran S. Wang and Jenny Y. Yang*

Department of Chemistry, University of California, Irvine, 92697

Table of Contents

General Methods: All synthesis and manipulations were carried out under an inert atmosphere of dinitrogen in a Vacuum Atmospheres OMNI-Lab glovebox or using standard Schlenk techniques. Organic solvents used during synthesis and/or manipulations were degassed by sparging with argon and dried by passing through columns of neutral alumina or molecular sieves and stored over activated 3 Å molecular sieves. Water was obtained from a Barnstead Nanopure filtration system and was degassed under active vacuum. All deuterated solvents were purchased from Cambridge Isotope Laboratories, Inc. Deuterated solvents used for nuclear magnetic resonance (NMR) spectroscopic characterization were degassed via three freeze-pump-thaw (FPT) cycles and stored over activated 3 Å molecular sieves prior to use. All solvents and reagents were purchased from commercial vendors and used without further purification unless otherwise noted. Electrochemical studies under pure CO_2 atmospheres were performed using ultra high purity (99.999%) CO_2 that was passed through a VICI carbon dioxide purification column to eliminate residual H_2O, O_2, CO, halocarbons, and sulfur compounds. Buffer pH levels were adjusted using concentrated solutions of Na_2CO_3, H_3PO_4, or by additional CO_2 bubbling and measured using a Thermo Scientific Orion Star A216 pH meter.

Physical Methods: ^1H and $^{31}P\{^1H\}$ nuclear magnetic resonance (NMR) spectra were collected at 298K, unless otherwise noted, on a Bruker AVANCE 600 MHz spectrometer equipped with a BBFO cryoprobe. Low temperature ^1H and $^{31}P\{^1H\}$ NMR spectra were collected on a Bruker DRX 500 MHz spectrometer equipped with a BBO probe. Chemical shifts are reported in δ units notation in parts per million (ppm). ^1H spectra are referenced to the residual solvent resonances of the deuterated solvent. $^{31}P\{^1H\}$ spectra were referenced to H_3PO_4 at 0 ppm within XwinNMR or Bruker's Topspin software, using the

known frequency ratios (Ξ) of the ^{31}P standard to the lock signal of the deuterated solvent or referenced to an external standard of triphenylphosphate in a capillary. Manual shimming, Fourier transformation, and automatic spectrum phasing were performed using Xwin-NMR software when using the 500 MHz spectrometer. Spectra were analyzed and figures were generated using MestReNova 6.0.2 software. Peak integrations were calculated within MestReNova. Quantitative ^{1}H NMR experiments for formate detection were performed with a delay time of 60s and acquisition time of 5s. Room temperature electronic absorption spectra were recorded using a 1 cm quartz cuvette with an Agilent Cary 60 UV-Vis spectrophotometer fitted with an Agilent fiber optic coupler connected to an Ocean Optics CUV 1 cm cuvette holder in a glovebox under an inert atmosphere of N_2.

Electrochemistry: All measurements were performed on a Pine Wavedriver 10 bipotentiostat. Cyclic voltammetry was performed with a 1 mm diameter glassy carbon disc working electrode, a glassy carbon rod counter electrode, and a saturated calomel electrode (SCE) reference electrode. Internal resistance was measured for each solution using a current interrupt method, and resistance manually compensated for between 80-90% of the measured value for each voltammogram performed. All experiments were performed in degassed aqueous solutions with 1 mM analyte and 0.4 M phosphate, bicarbonate, or carbonate buffer with the buffer acting as supporting electrolyte. Samples for electrochemical studies performed under CO_2 atmosphere were prepared by sparging the analyte solution with solvent saturated carbon dioxide gas prior to measurement and the headspace above the solution was blanketed with CO_2 during each measurement. Controlled potential electrolysis experiments were performed in a custom H-cell with the working and counter compartments (16.1 and 8.0 mL respectively) separated by a medium

porosity glass frit. The working and counter compartments were sealed with GL25 and GL18 open top caps with silicone/PTFE septa from Ace Glass. The working compartment contained: 2.0 mM catalyst, 0.2 M carbonate buffer, a glassy carbon rod working electrode, the SCE reference electrode, and a mercury pool at the bottom of the compartment. The counter compartment contained an aqueous solution of 0.2 M carbonate buffer and a 1" x 2.25" piece of carbon fabric as the counter electrode. After the electrolysis period, the volume in the working compartment was measured. The formate concentration was determined by ^{1}H NMR after addition of an internal standard (sodium propane sulfonate) to a known volume of electrolysis solution. The headspace of the working compartment was sampled with a Restek A-2 Luer lock gas-tight syringe. Headspace hydrogen was quantified by gas chromatography on an Agilent 7890B instrument with a HP-PLOT Molesieve column (19095P-MS6, 30m x 0.530 mm, 25 μm) and TCD detector.

Synthesis of $[Co(dmpe)_2(H)_2][BF_4]$ (1): Precursor $[Co(dmpe)_2(MeCN)_2][BF_4]_2$ was synthesized per the literature procedure[1] and recrystallized by vapor diffusion of diethyl (Et_2O) into an acetonitrile solution (MeCN). The coordinated solvent was removed from the recrystallized material *in vacuo* to obtain $[Co(dmpe)_2][BF_4]_2$ as a green solid. $[Co(dmpe)_2][BF_4]_2$ (171 mg, 0.320 mmol) was dissolved in 20 mL of cold MeCN at –40°C in a 250 mL Schlenk flask, forming a dark red-brown solution of $[Co(dmpe)_2(CH_3CN)_2][BF_4]_2$ *in situ*. To this stirring solution, a yellow solution of 1.1 eq of $Co(C_5(CH_3)_5)_2$ (118 mg, 0.358 mmol) dissolved in 20 mL of cold THF at –40°C was added dropwise. The mixture was warmed to room temperature and the brownish-red solution turned yellow after addition of H_2. The solvent was removed, and the solids were extracted with THF followed by filtration through Celite. The crude product precipitated as a white powder after

concentration of the THF filtrate (~3 mL) and addition of excess pentane. The powder was isolated by filtration through Celite before being redissolved in a minimal amount of THF. Off-white crystals were grown by successive recrystallizations from vapor diffusion of diethyl ether into THF (62 mg, 43% yield, first crop). $^{31}P\{^{1}H\}$ and ^{1}H NMR spectra match those previously published.

NMR characterization of $[Co(dmpe)_2(H)_2][BF_4]$ (1)

As previously reported, the $^{31}P\{^{1}H\}$ spectrum for $[Co(dmpe)_2(H)_2][BF_4]$ has two characteristic broad peaks at room temperature likely due to the fluxionality of the dmpe ligands.[2] The broadness may also be attributed to *cis-trans* isomerization or quadrupolar coupling to the ^{59}Co nucleus.[3,4] Low temperature ^{31}P and $^{31}P\{^{1}H\}$ spectra were obtained in an attempt to further characterize $[Co(dmpe)_2(H)_2][BF_4]$ and measure the ^{31}P-^{1}H coupling with the hydride. When cooled to 183K, the peaks sharpen, suggesting that the ligands are less fluxional than at room temperature (**Figure S1**). However, even at 183K, both the $^{31}P\{^{1}H\}$ and ^{31}P spectra look similar – no ^{31}P-^{1}H coupling is observed in the phosphorus spectrum even in the absence of ^{1}H decoupling (**Figure S2**).

At 183K, the hydride peak of $[Co(dmpe)_2(H)_2][BF_4]_2$ resolves into a multiplet in the ^{1}H NMR at -14.4 ppm (**Figure S3**). At 183K, $^{1}H\{^{31}P\}$ experiments show that the multiplet for the hydride peak at -14.4 ppm collapses into a singlet when the decoupling is irradiated at 58.5 ppm in the ^{31}P spectrum (**Figure S4**), suggesting that the splitting normally observed in the ^{1}H spectrum does arise from ^{31}P-^{1}H coupling. The magnitude of this coupling is likely too small to observe in the ^{31}P spectrum since the broad ^{31}P feature is 2 ppm wide while the widest expected doublet (J = 93 Hz) would result in a peak separation of 0.38ppm.

Calculation of overpotential

We report our overpotential as the difference between the applied potential during electrolysis and the thermodynamic potential of the reduction of CO2 to formate.[5]

$$CO_2(g) + 2\,e^- + H^+ \rightleftharpoons HCO_2^-(aq) \qquad E^{\circ'} = -0.43\,V\ vs.\ NHE\ @\ pH\ 7 \qquad \text{(Eq S1)}$$

$$CO_2(g) + 2\,e^- + H^+ \rightleftharpoons HCO_2^-(aq) \qquad E^{\circ'} = -0.46\,V\ vs.\ NHE\ @\ pH\ 8 \qquad \text{(Eq S2)}$$

Since the reaction of interest is a $2\,e^-/H^+$ process, the thermodynamic potential shifts by 30 mV/pH unit at these conditions.

For $[Co(dmpe)_2(OH)H]^+$, the applied potential of -1.50 V vs. SCE corresponds to -1.26 V vs. NHE.[6] At pH 8 which is approximately where formate selectivity is highest, the difference between the applied potential and the thermodynamic potential is 800 mV.

For $[Fe_4N(CO)_{12}]^-$, the applied potential of -1.20 V vs. SCE corresponds to -0.96 V vs. NHE.[7] At pH 7, the difference between the applied and thermodynamic potential is 530 mV. At pH 8, the difference is 500 mV.

For Ir(POCOP), the applied potential for the highest formate selectivity was -1.41 V vs. NHE, which corresponds to an overpotential of 950 mV between the applied and thermodynamic potentials at pH 7. Electrolysis at other pH conditions was not reported.[8]

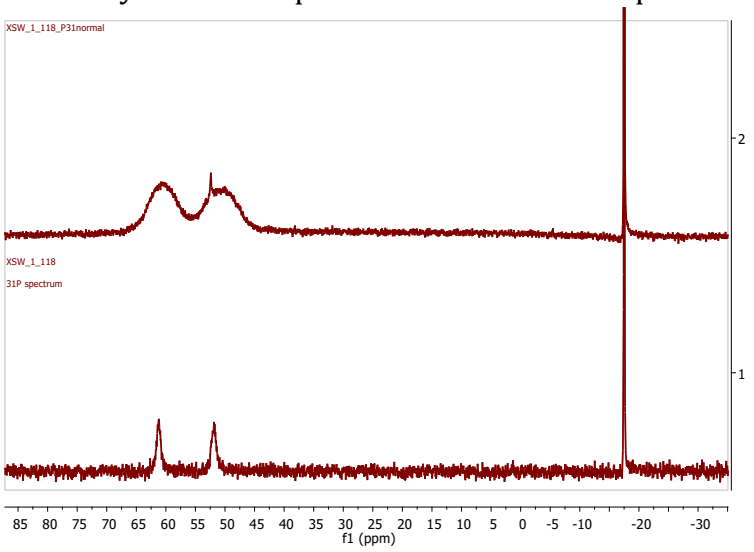

Figure S1. *Top:* $^{31}P\{^{1}H\}$ spectra of $[Co(dmpe)_2(H)_2][BF_4]$ (**1**) in THF at 298K, referenced to an external standard of triphenylphosphate. *Bottom:* $^{31}P\{^{1}H\}$ spectra of $[Co(dmpe)_2(H)_2][BF_4]$ (**1**) in THF at 183K, referenced to an external standard of triphenylphosphate.

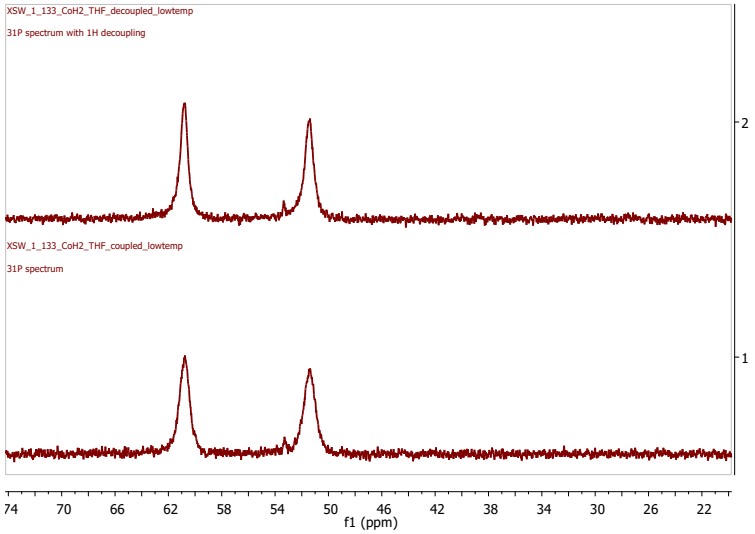

Figure S2. *Top*: $^{31}P\{^{1}H\}$ spectrum of $[Co(dmpe)_2(H)_2][BF_4]$ (**1**) at 183 K with a small impurity at 52.4 ppm in THF, referenced to an external standard of triphenylphosphate. *Bottom*: ^{31}P spectrum of $[Co(dmpe)_2(H)_2][BF_4]$ (**1**) at 183 K, referenced to an external standard of triphenylphosphate.

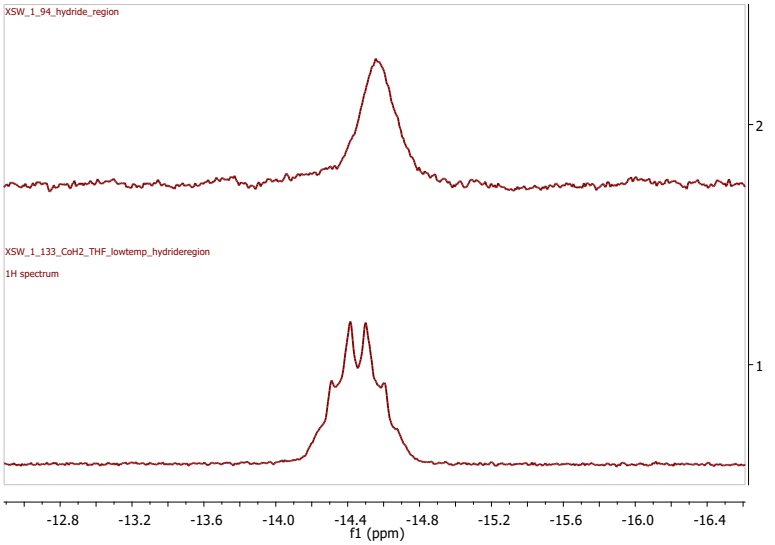

Figure S3. *Top*: Hydride region of ^{1}H spectrum of $[Co(dmpe)_2(H)_2][BF_4]$ (**1**) at 298K. *Bottom*: Hydride region of ^{1}H spectrum of $[Co(dmpe)_2(H)_2][BF_4]$ (**1**) at 183 K.

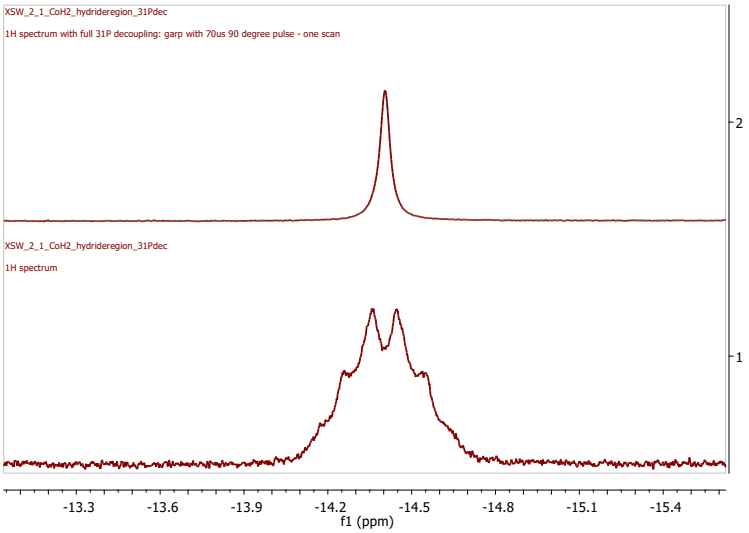

Figure S4. *Top*: Hydride region of ^{1}H spectrum of $[Co(dmpe)_2(H)_2][BF_4]$ (**1**) at 183 K with ^{31}P decoupling at 58 ppm. *Bottom*: Hydride region of ^{1}H spectrum of $[Co(dmpe)_2(H)_2][BF_4]$ (**1**) at 183 K with no decoupling.

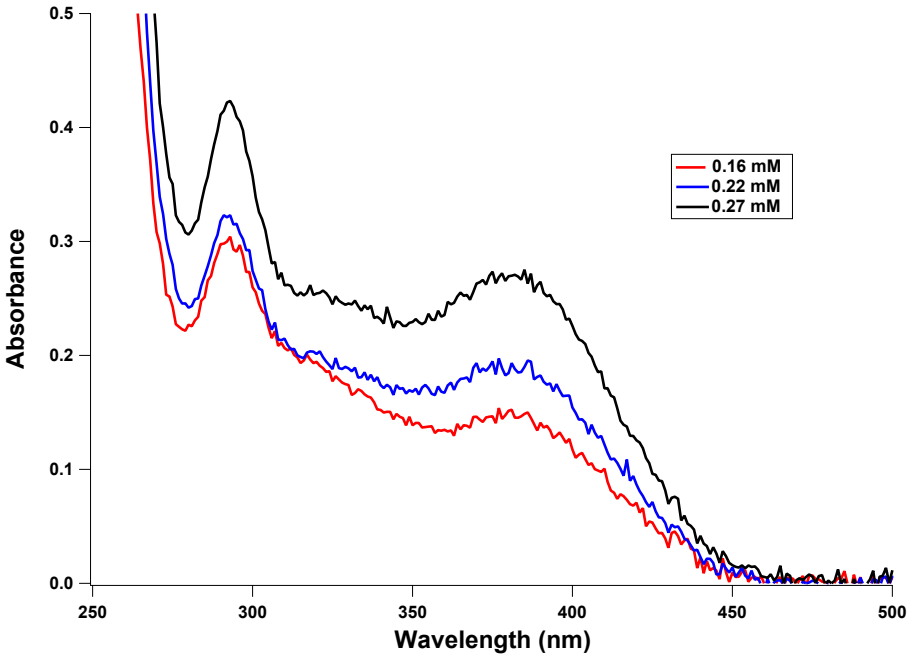

Figure S5. UV-Vis spectra of increasing amounts of $[Co(dmpe)_2(H)_2][BF_4]$ (**1**) in 0.2 M phosphate buffer used to calculate ε from the Beer-Lambert law (A = εbc where b = 1cm and c = concentration in M). $[Co(dmpe)_2(H)_2][BF_4]$ (**1**) has two features in the UV-Vis spectrum: a broad peak at 385 nm with ε = 1064 $M^{-1}cm^{-1}$ as well as a sharper peak at 293 nm with ε = 1098 $M^{-1}cm^{-1}$.

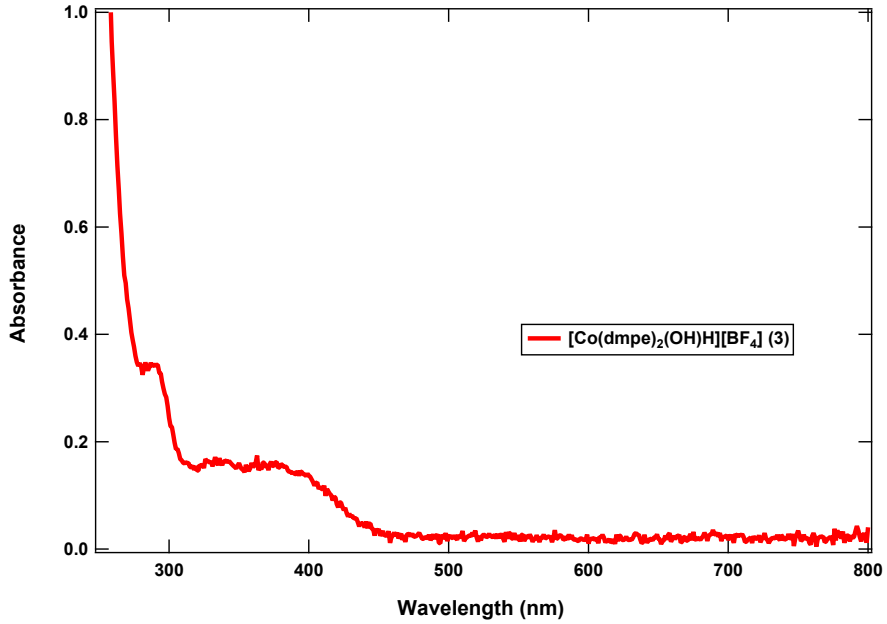

Figure S6. UV-Vis spectrum of a 0.20 mM solution of $[Co(dmpe)_2(OH)H][BF_4]$ (**3**) in 0.2 M phosphate buffer. $[Co(dmpe)_2(OH)H][BF_4]$ (**3**) has two features in the UV-Vis spectrum: a very broad peak at 376 nm, and a sharper peak at 291 nm.

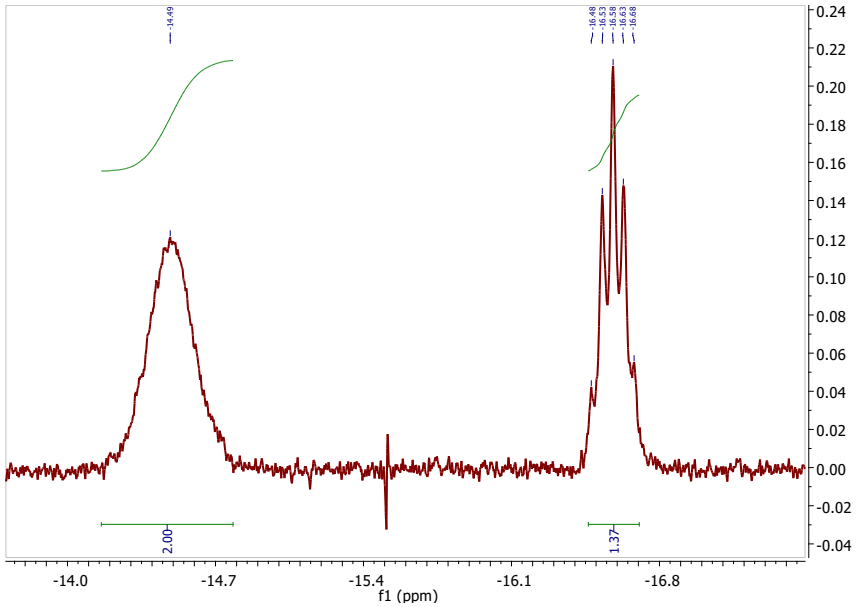

Figure S7. ^{1}H spectrum taken in d_8-THF showing the hydride region and product distribution between $[Co(dmpe)_2(H)_2]^+$ and $Co(dmpe)_2H$ after $[Co(dmpe)_2(H)_2]^+$ was placed in pH 13.3 phosphate buffer (0.4 M) for 96h. Due to the insolubility of $Co(dmpe)_2H$ in H_2O, NMR spectra were acquired in THF.

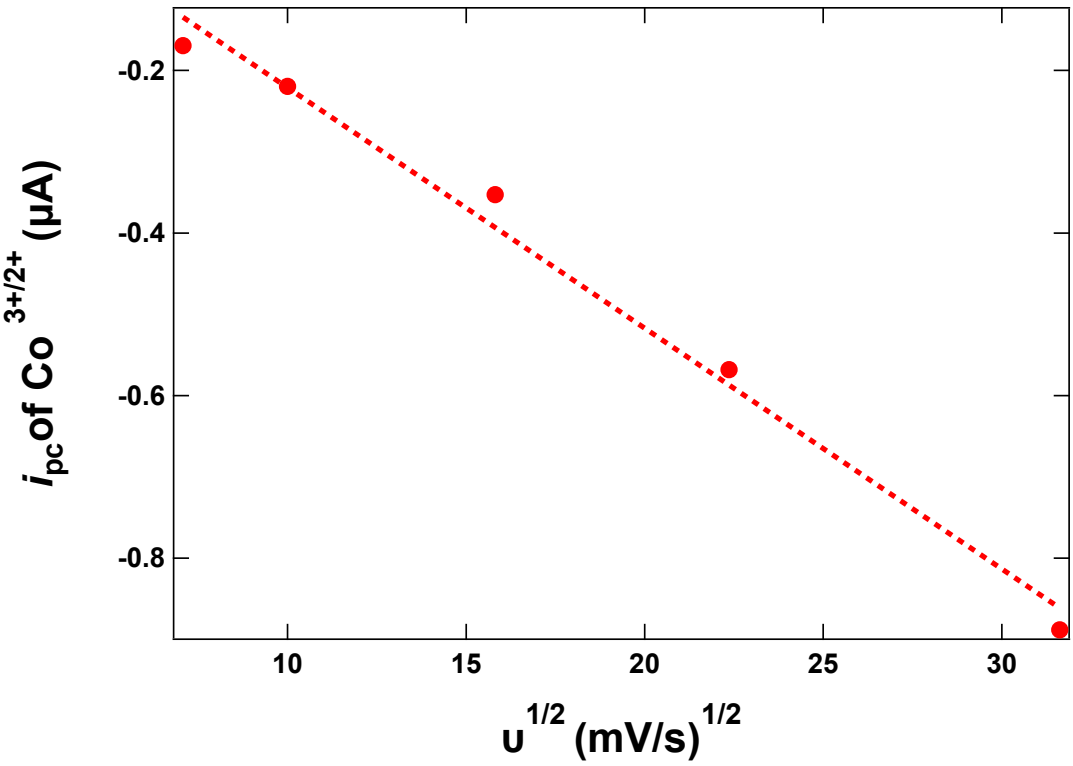

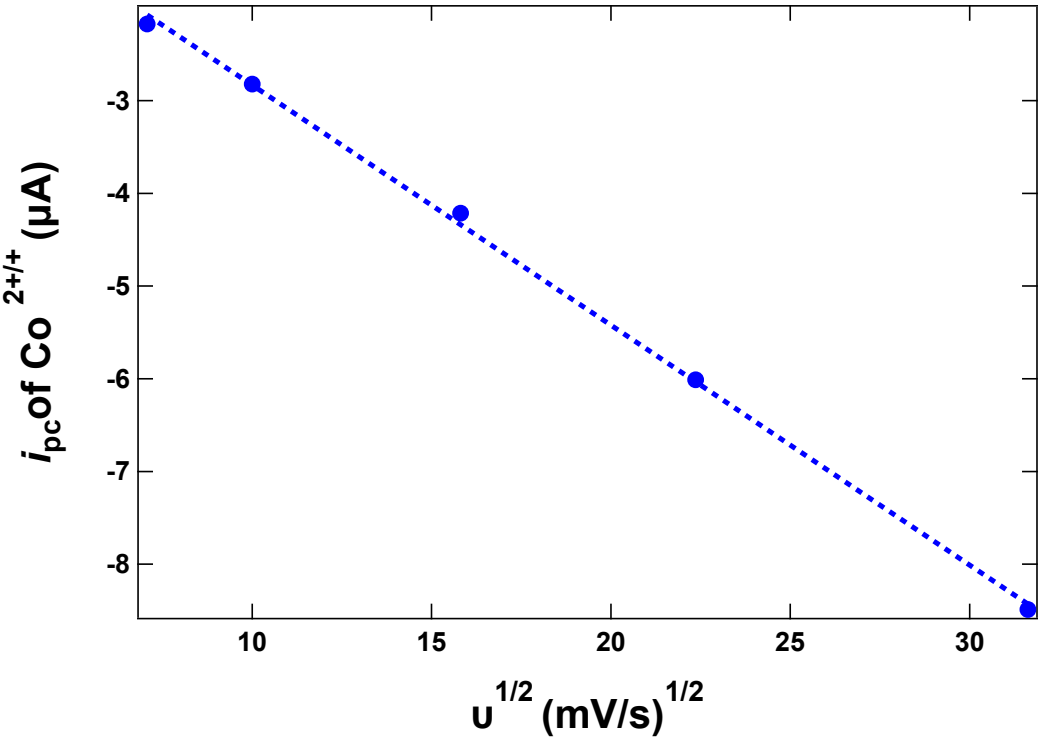

Figure S8. Top: Variable scan rate plot of i_{pc} of the $Co^{3+/2+}$ feature of $[Co(dmpe)_2(OH)H]^+$ from 50 mV/s to 1000 mV/s. R^2 = 0.989. Bottom: Variable scan rate plot of i_{pc} of the $Co^{2+/+}$ feature of $[Co(dmpe)_2(OH)H]^+$ from 50 mV/s to 1000 mV/s. R^2 = 0.999 Plots show a linear relationship with the square root of scan rate, indicating that the species is freely diffusing in solution.

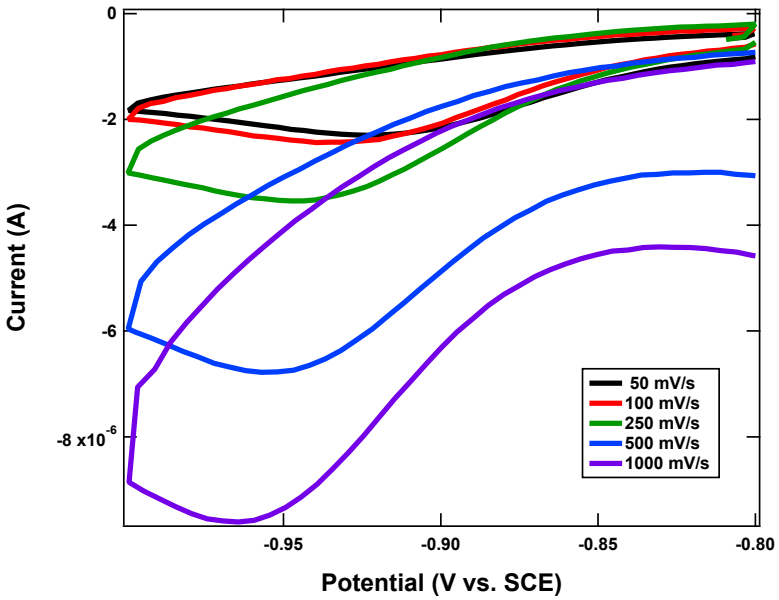

Figure S9. Cyclic voltammograms of the $Co^{3+/2+}$ couple of $[Co(dmpe)_2(OH)H]^+$ in bicarbonate buffer under N_2 (pH 9.9) do not show reversibility at faster scan rates.

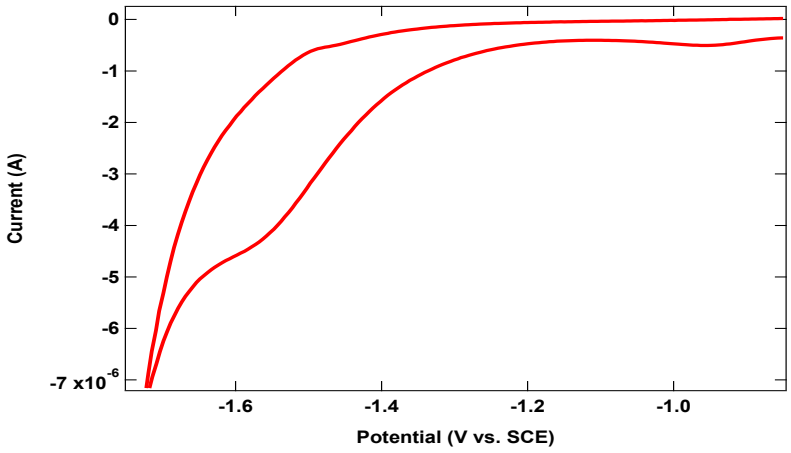

Figure S10. Cyclic voltammogram of 1 mM $[Co(dmpe)_2(OH)H]^+$ in 0.4 M bicarbonate buffer (pH 9.9) at 250 mV/s using a glassy carbon disk working electrode.

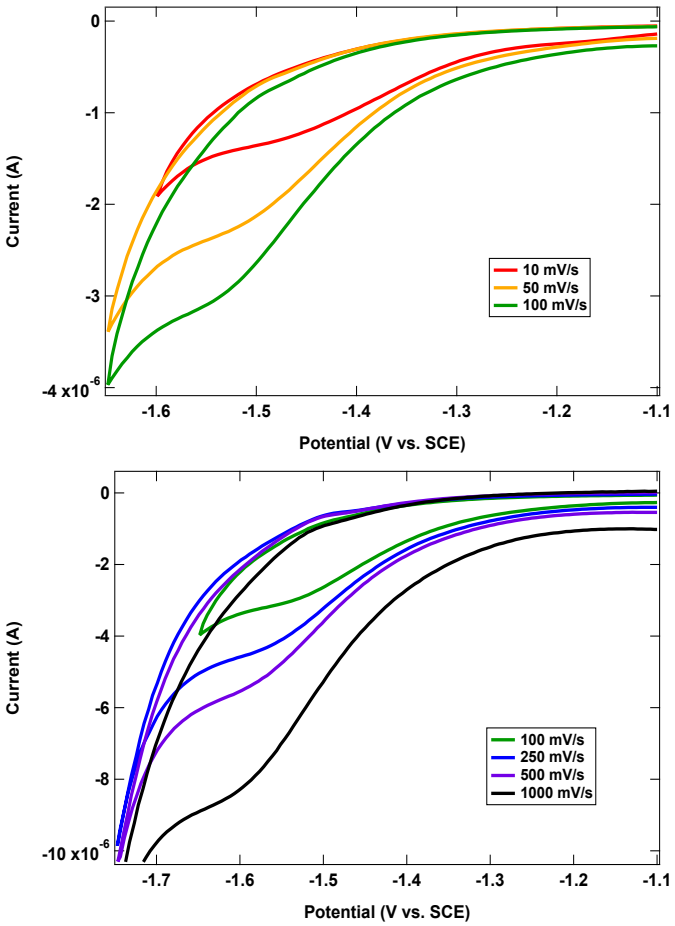

Figure S11. For the $Co^{2+/+}$ couple of $[Co(dmpe)_2(OH)H]^+$ in bicarbonate buffer (pH 9.9), an oxidation event at -1.48 V is not observed at slow scan rates below 100 mV/s (*top*) but is observed when scanning at 100 mV/s and above (*bottom*).

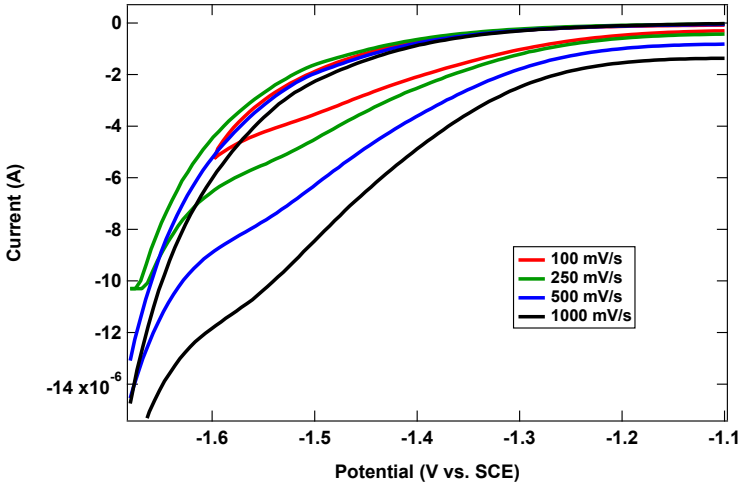

Figure S12. No oxidation peak at -1.48 V is observed for $[Co(dmpe)_2(OH)H]^+$ after CO_2 addition (pH 7.9), even at fast scan rates.

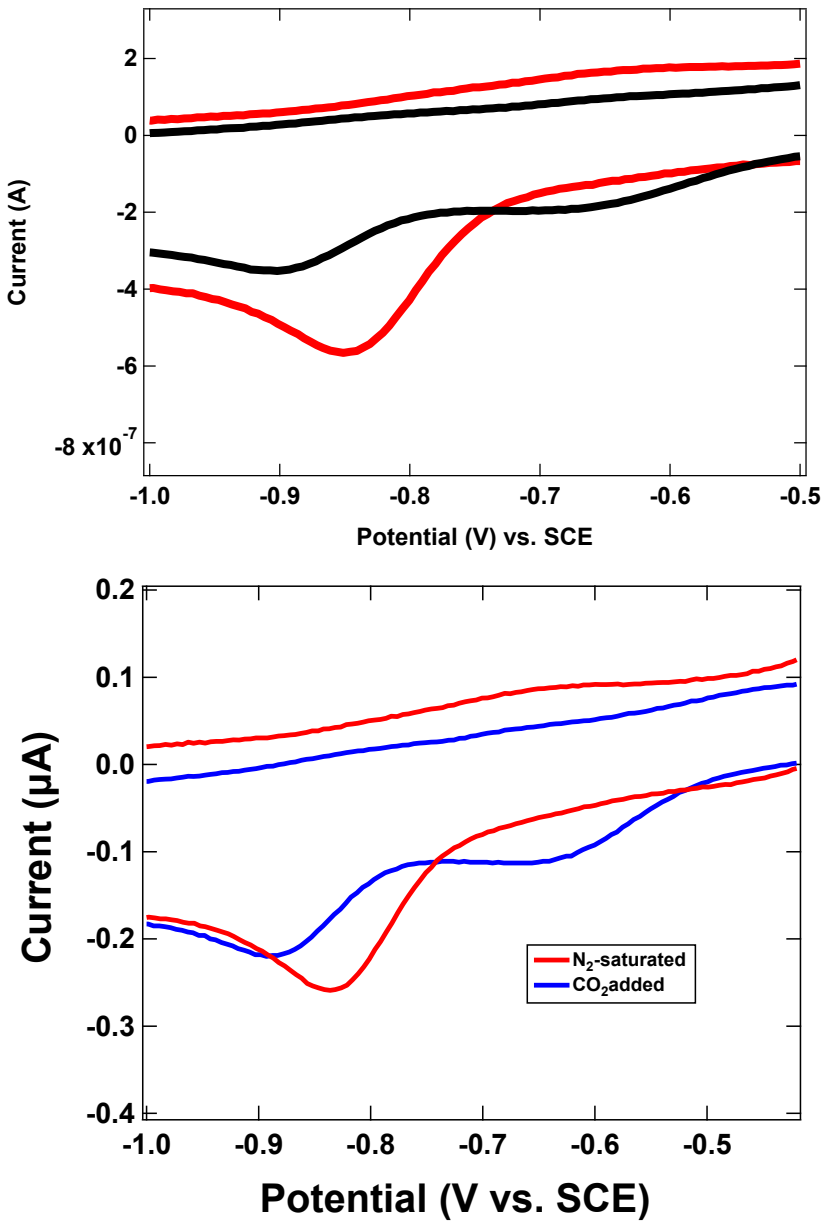

Figure S13. **Top**: Cyclic voltammograms of $[Co(dmpe)_2(OH)H]^+$ in 0.4 M phosphate buffer at pH 7.9 (red) and 0.4 M bicarbonate buffer at pH 9.9 (black) showing an additional redox event at –0.62 V vs. SCE in bicarbonate buffer which is not observed in phosphate buffer. **Bottom**: Cyclic voltammograms of $[Co(dmpe)_2(OH)H]^+$ in 0.4 M phosphate buffer at pH 7.9 under N_2 (red) and CO_2 (blue) showing an additional redox event at –0.62 V vs. SCE after CO_2 addition which is not observed under N_2. Experiments were conducted using a glassy carbon working electrode and scanned at 250 mV/s.

Table S1. Summary of CPE data using a mercury pool working electrode.

	Charge passed (C)	H_2 (mmol)	HCO_2^- (mmol)	Faradaic yield (% H_2)	Faradaic yield (% HCO_2^-)
pH 7.9	0.82	0.0026	0.0015	62	36
pH 8.1	0.74	0.0029	Not detected	70	N/A

Experiments were conducted with 2 mM of analyte (0.015 mmol) using a mercury pool working electrode, a carbon fabric counter electrode, and a SCE reference electrode in 0.2 M CO_2-saturated carbonate buffer. The mercury pool working electrode was created by submerging a 1 mm glassy carbon disk electrode into a 1 mL pool of mercury at the bottom of a customized H-cell. The solutions were electrolyzed at -1.50 V vs. SCE for 6 h over a mercury pool. H_2 was quantified by GC, while formate was quantified by ^{1}H NMR using an internal reference.

References

(1) Mock, M. T.; Potter, R. G.; O'Hagan, M. J.; Camaioni, D. M.; Dougherty, W. G.; Kassel, W. S.; DuBois, D. L. Synthesis and Hydride Transfer Reactions of Cobalt and Nickel Hydride Complexes to BX3 Compounds. *Inorg. Chem.* **2011**, *50* (23), 11914–11928. https://doi.org/10.1021/ic200857x.

(2) García Basallote, M.; L. Hughes, D.; Jiménez-Tenorio, M.; Jeffery Leigh, G.; Puerta Vizcaíno, M. C.; Valerga Jiménez, P. Chemistry of Cobalt Complexes with 1,2-Bis-(Diethylphosphino)Ethane: Hydrides, Carbon Disulfide Complexes, and C–H Cleavage in Activated Alk-1-Ynes. Crystal Structure of [CoH(C[Triple Bond, Length Half m-Dash]CCO 2 Et)(Et 2 PCH 2 CH 2 PEt 2) 2][BPh 4]. *J. Chem. Soc. Dalton Trans.* **1993**, *0* (12), 1841–1847. https://doi.org/10.1039/DT9930001841.

(3) Jewiss, H. C.; Levason, W.; Webster, M. Coordination Chemistry of Higher Oxidation States. 20. Synthesis and Cobalt-59 NMR Studies of Tris(Diphosphine)Cobalt(3+), Tris(Diarsine)Cobalt(3+) and Related Complexes. Crystal Structure of Tris[o-Phenylenebis(Dimethylarsine)]Cobalt(III) Tetrafluoroborate-2-Water. *Inorg. Chem.* **1986**, *25* (12), 1997–2001. https://doi.org/10.1021/ic00232a019.

(4) Jessop, P. G.; Joó, F.; Tai, C.-C. Recent Advances in the Homogeneous Hydrogenation of Carbon Dioxide. *Coord. Chem. Rev.* **2004**, *248* (21), 2425–2442. https://doi.org/10.1016/j.ccr.2004.05.019.

(5) Appel, A. M.; Bercaw, J. E.; Bocarsly, A. B.; Dobbek, H.; DuBois, D. L.; Dupuis, M.; Ferry, J. G.; Fujita, E.; Hille, R.; Kenis, P. J. A.; Kerfeld, C. A.; Morris, R. H.; Peden, C. H. F.; Portis, A. R.; Ragsdale, S. W.; Rauchfuss, T. B.; Reek, J. N. H.; Seefeldt, L. C.; Thauer, R. K.; Waldrop, G. L. Frontiers, Opportunities, and Challenges in Biochemical and Chemical Catalysis of CO_2 Fixation. *Chem. Rev.* **2013**, *113* (8), 6621–6658. https://doi.org/10.1021/cr300463y.

(6) Bard, A., J.; Faulkner, L. R. *Electrochemical Methods: Fundamentals and Applications*, 2nd ed.; John Wiley & Sons, Inc., 2001.

(7) Taheri, A.; Thompson, E. J.; Fettinger, J. C.; Berben, L. A. An Iron Electrocatalyst for Selective Reduction of CO_2 to Formate in Water: Including Thermochemical Insights. *ACS Catal.* **2015**, *5* (12), 7140–7151. https://doi.org/10.1021/acscatal.5b01708.

(8) Kang, P.; Meyer, T. J.; Brookhart, M. Selective Electrocatalytic Reduction of Carbon Dioxide to Formate by a Water-Soluble Iridium Pincer Catalyst. *Chem. Sci.* **2013**, *4* (9), 3497–3502. https://doi.org/10.1039/C3SC51339D.